Research Square

Preprints are preliminary reports that have not undergone peer review.
They should not be considered conclusive, used to inform clinical practice,
or referenced by the media as validated information.

Hybrid Energy Source Fed Hystersis Current Control Algorithm for Cascaded Multi Level Inverter

Vinothini Jayaprakasam

vinovenba19@gmail.com

Dhanalakshmi Srinivasan University

Ramkumar Ravindran

Dhanalakshmi Srinivasan University

Ravi S

Research Article

Keywords: Multilevel Inverter (MLI), Perturb and Observe (P&O), Maximum power point tracking (MPPT) algorithm, Hysteresis current control (HCC), Photo voltaic system (PV)

Posted Date: March 16th, 2026

DOI: https://doi.org/10.21203/rs.3.rs-8861291/v1

License: This work is licensed under a Creative Commons Attribution 4.0 International License.
Read Full License

Additional Declarations: No competing interests reported.

HYBRID ENERGY SOURCE FED HYSTERSIS CURRENT CONTROL ALGORITHM FOR CASCADED MULTI LEVEL INVERTER

Jayaprakasam Vinothini [1], Ravindran Ramkumar [2]*, Ravi S[3]*

Research Scholar, Department of Electrical and Electronics Engineering, School of Engineering and Technology, Dhanalakshmi Srinivasan University, Tiruchirappalli, India.

Email Id: vinovenba19@gmail.com

Associate Professor, Department of Electrical and Electronics Engineering, School of Engineering and Technology, Dhanalakshmi Srinivasan University, Tiruchirappalli, India.

Email Id: 2019ramkr@gmail.com*

Professor, Department of Electrical Engineering, Faculty of Engineering, Hormuud University, Mogadishu, Somalia.

Email Id: ravi@huweb.hu.edu.so*

Ravindran Ramkumar [2]*Corresponding Author, Ravi S[3]* Corresponding Author

ABSTRACT

In this work Hybrid energy fed cascaded multilevel inverter is implemented and controlled using Hysteresis Current Control algorithm (HCC), which improves the inverter output voltage, reduces THD and minimizes the common mode voltage, which is lowered to Vdc/2 times the applied DC input voltage. A modified variable step size P&O MPPT algorithm is developed in this work, which can improve the PV system's dynamic and steady state performance at the same time. Traditional P&O MPPT has limitations, which are addressed by the suggested variable step size technique. In this system results are evaluated through MATLAB/Simulink platform.

Keywords: Multilevel Inverter (MLI), Perturb and Observe (P&O), Maximum power point tracking (MPPT) algorithm, Hysteresis current control (HCC), Photo voltaic system (PV).

INTRODUCTION

In the long run, fossil fuels will be unable to provide long-term energy demands, and the void they leave behind will have to be supplied by alternating sources of energy. Wind and solar energy, for example, are abundant sources of sustainable energy. Because oil and gas prices fluctuate, but the operating and maintenance costs of renewable systems are free, the cost of power generated can be assumed to remain steady for a length of time. [1]-[4] These distributed power generation systems (DPGS) can be positioned near to the load, reducing transmission losses in the traditional transmission and distribution system. [5]

Multilevel inverters are often used in high-power and medium-voltage applications. To provide high power, multilevel inverters use a series of power semiconductor switches with numerous low-voltage DC sources to generate staircase output voltage levels. Multilevel inverters can use fuel cells, batteries, capacitors, PV cells, wind energy, and other renewable sources as multiple DC sources. [6]-[9] The DC supply voltage ratings are used to design the ratings of power semiconductor devices. [10] Reduction of harmonics, almost sinusoidal output, and electromagnetic interference concerns, voltage balancing and common mode voltage are all possible with multilevel inverters. [12]

The inverter level is determined by the number of bridges and power semiconductor switches connected in the system, with each bridge circuit having its own DC source. [11] Voltage unbalance is one of the key drawbacks of cascaded multilayer inverters. In comparison to other topologies, the PWM control technique necessitates a greater number of power semiconductor switches. [13]-[15]

Some of the pulse width modulation techniques that are expected for multilevel converters are Space Vector Pulse Width Modulation, hysteresis control, sinusoidal pulse width modulation, maximum boost control, and selective

harmonic elimination [17]. To operate the cascaded inverter, a new hysteresis reactive current algorithm is utilized, which enhances overall harmonic distortion and solves synchronization issues between the inverter and the grid system. [16]

Overall harmonic distortion is reduced more effectively by the suggested photovoltaic-wind hybrid energy system with cascading multilevel inverters than by the IEEE standard. It is proposed that a hysteresis current control technology be used to improve output voltage and current control. Closed loop control is employed to meet the system's power requirements, which are met by photovoltaic-wind hybrid energy system. [18]

A five-level single-phase cascaded multilevel converter with two separate DC sources is powered by a photovoltaic-wind hybrid energy source. The suggested hysteresis current controller balances and standardizes the voltages across each DC source. The performance of STATCOM is evaluated in both steady and dynamic states by connecting it to a grid-connected system. Closed loop hysteresis current control is performed using a PLL and a PI controller to reduce Total Harmonic Distortion (THD) and enhance output voltage. [19]-[20]

The following are some of the paper highlights:

- CMV is reduced to a minimum of 122.7 V, which is $V_{dc}/2$ times the input voltage (245.4 V).
- The output voltage has a THD of 7.12 percent and the output current has a THD of 8.98 percent.
- The updated variable step size P&O MPPT algorithm has been presented, which can effectively increase the PV system's dynamic and steady state performance.

HYBRID ENERGY SOURCE FOR CASCADED MULTI LEVEL INVERTER SYSTEM

Photovoltaic Source

The photovoltaic effect, which occurs when incident radiation energy exceeds the semiconductor device's threshold junction voltage, transforms solar energy into electricity in a PV cell or array. If a circuit is clogged, the electrons will attract this energy and create current. Because a single cell's output is on the scale of a few mill amperes, PV arrays are made up of multiple such cells. The voltage is increased when arrays are connected in series, while the current is increased when they are connected in parallel. A current source in tandem with a diode is a simple model of a PV cell.

Wind Energy System

Wind flows as a result of pressure differences caused by the sun's non-uniform heating of the surface air. The kinetic energy of the wind is used to turn the turbine rotor mechanically, and the turbine blades encounter rotating torque, which causes rotation and axial drive, which the structure must endure.

The mechanical energy output of the turbine is dictated by the wind speed and pressure drop as the wind loses kinetic energy as it goes through the rotor.

In this variant of WECS, the wind turbine is linked to a permanent magnet synchronous generator by a shared shaft, which creates torque for the generator based on wind speed. Permanent magnets are a potential choice for the generator's rotor due to advancements in magnetizing capabilities and accessibility. Losses are also kept to a minimum because there is no excitation current and thus no excitation losses. If the number of poles on the machines is great enough, the gearbox requirement can be eliminated. However, if the harmonic level is not regulated, the permanent magnet synchronous generator output contains many harmonics that might destabilize not only the inverter's operation but also put sensitive equipment at risk. For these reasons, we employ a diode rectifier to convert the PMSG's ac voltage to dc. The

conventional three phase full wave AC-DC converter with Diode Bridge is utilized as the diode rectifier. The photovoltaic and rectified permanent magnet synchronous generator outputs are combined, and the accumulated voltage is fed into a single-phase, cascading multilevel inverter. [4]

Modified Perturb and Observe (P&O) MPPT Algorithm

The most widely used MPPT algorithm is the (P & O) algorithm. It does, however, have several drawbacks, such as oscillations around the MPP and a poor response time. The tracker works on a regular basis, comparing the current value of the power to the previous value to identify the change in the solar array voltage or current (incrementing or decrementing) (depending on the control strategy). If the PV generator's voltage is disrupted in one direction and $dP/dV > 0$, the algorithm P & O may continue to disrupt the PV voltage in that direction. If $dP/dV = 0$, the MPP is overrun, and the P & O algorithm changes the disturbance's direction. The most widely used MPPT algorithm is the (P & O) algorithm. It does, however, have several drawbacks, such as oscillations around the MPP and a poor response time. The tracker works on a regular basis, comparing the current value of the power to the previous value to identify the change in the solar array voltage or current (incrementing or decrementing) (depending on the control strategy). [6]

The conventional P&O method is incapable of meeting both the performance objectives of fast dynamic reaction and acceptable accuracy in the steady state. This is due to the fact that if the step-size is large enough for a fast-dynamic reaction, the oscillation around the maximum-power operating point will grow during the steady state, resulting in decreased power generation. The goal of the new strategy is to find an effective way to improve both dynamics and steady state performance. Figure 1 depicts the new method's principle. [9]

The novel approach is significantly faster and more precise than existing fixed-step-size algorithms. The proposed method's algorithm is depicted

in Figure 3 as a flowchart.

The proposed method in Figure. 2 (b) can converge to MPP more quickly than the P&O method in Figure. 2 (a). The P&O method is limited by its step size; a large step size leads to rapid dynamics but also to excessive steady-state oscillations, resulting in a low efficiency. [10]

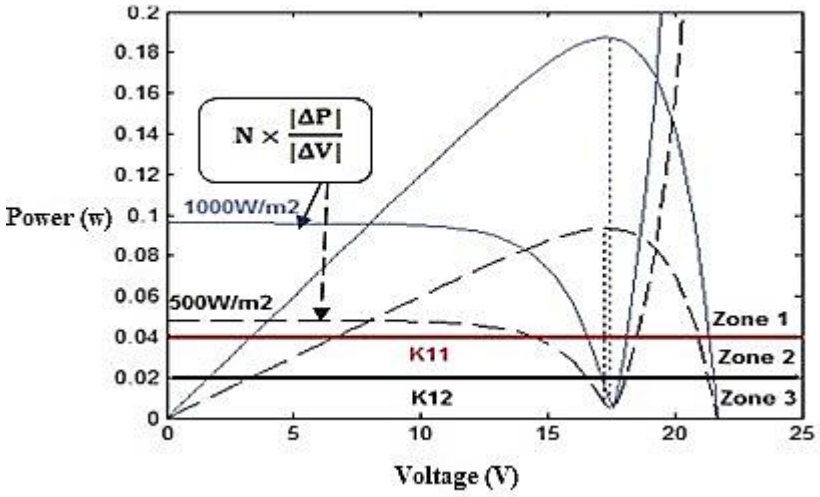


Figure 1 Concept of modified P & O algorithm

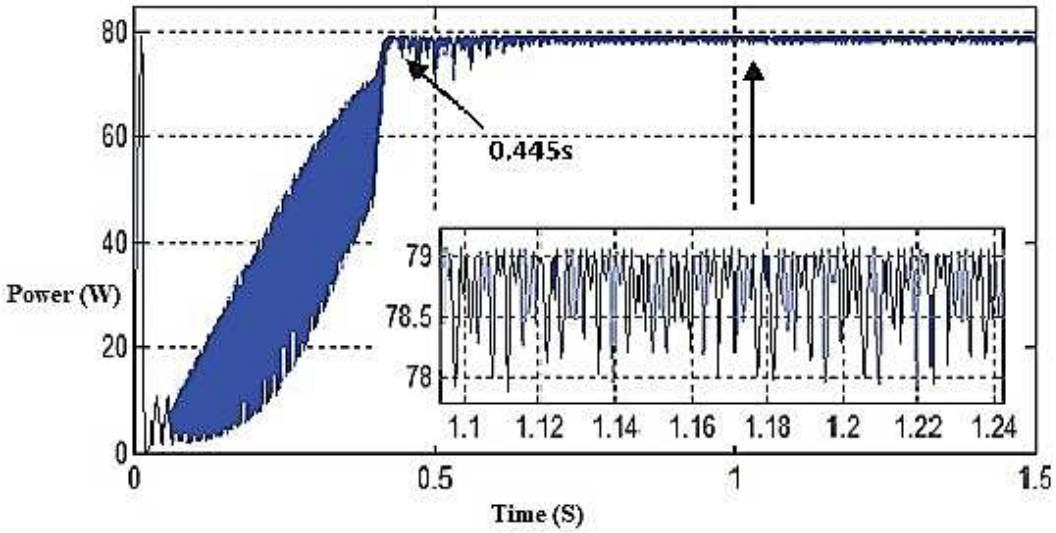
Furthermore, when the MPPT is run with a reduced step size, the situation is inverted. However, compared to the P&O approach with fixed step sizes, the proposed method has a larger step size while far away from MPP to acquire a rapid response speed and a small step size at the maximum power point to obtain improved steady-state qualities. [12]

The suggested method's output power could eventually converge to MPP in 0.13s. The P&O technique, on the other hand, converges to MPP in 0.445s. MPP tracking takes longer with the P&O technique.

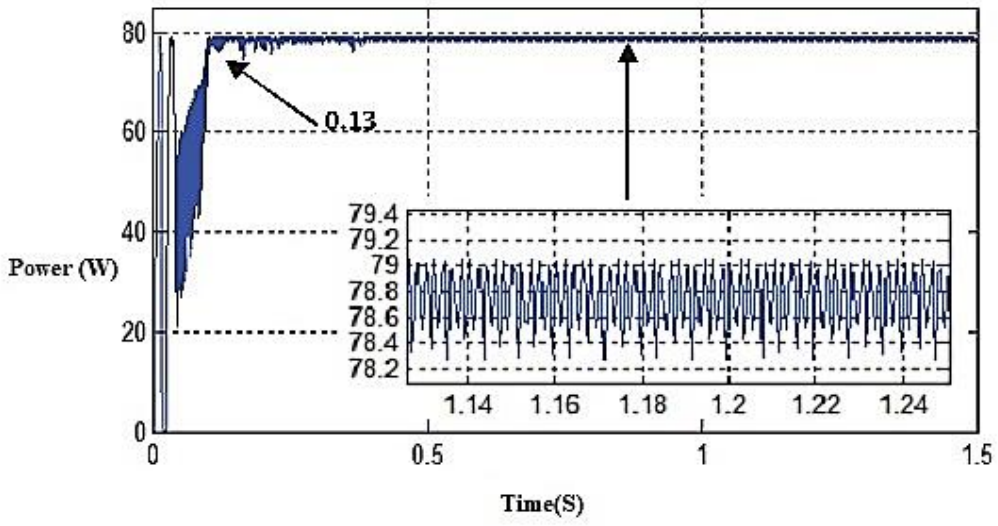
The updated P&O method compares two fixed values (K11 and K12) and generates a variable step size. The MPPT with a variable step size has high dynamic performance but fewer steady oscillations. The dynamic performance is

superior to the fixed step size performance.

A modified variable step size P&O MPPT algorithm has been given in this research, which can improve the PV system's dynamic and steady state performance at the same time. Traditional P&O MPPT has limitations, which are addressed by the suggested variable step size technique.



(a)



(b)

Figure 2 Output power of PV (a) Conventional P&O method and (b) Modified P & O method

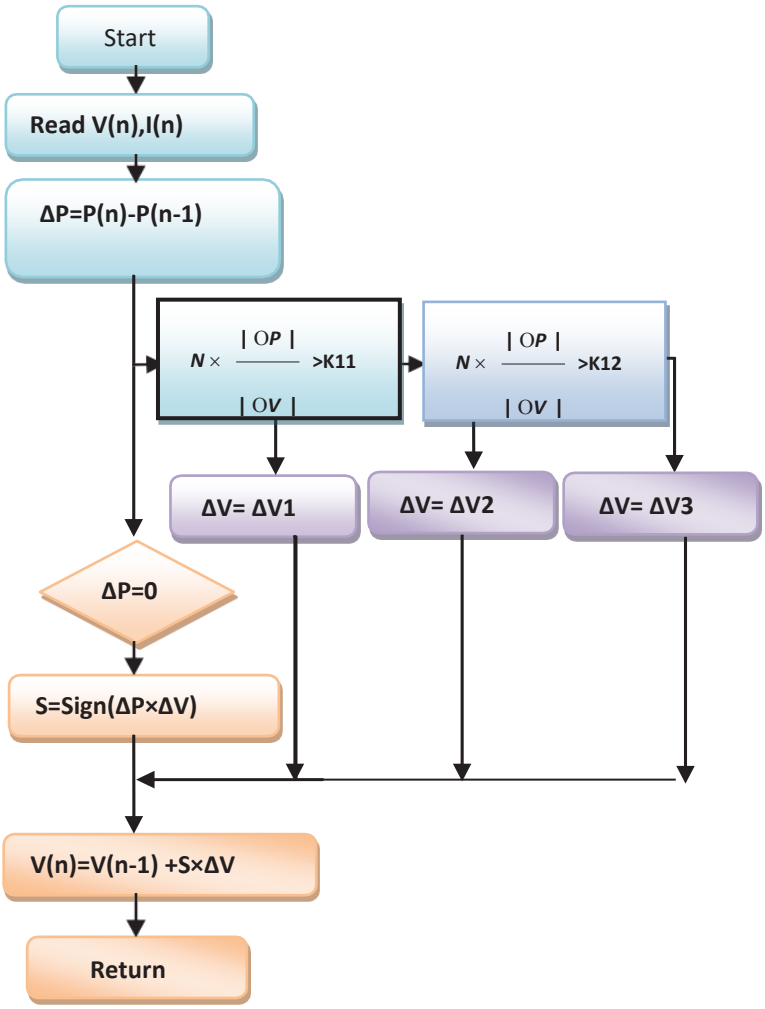


Figure 3 Flow chart of modified P &O algorithm

CONFIGURATION OF SUGGESTED CASCADED MULTI LEVEL INVERTER SYSTEM

A single phase five levels cascaded multilevel inverter is used to build the STATCOM model. When the number of levels in a multilevel inverter system grows, so does the number of power electronic switching devices and other equipment, and the inverter's structure becomes more complicated. A complex controller with an adequate switching gate drive circuit is required to manage and coordinate the switching devices and voltage level.

When the number of levels in a system grows, so does the number of

voltage sources used, resulting in a voltage imbalance among the system's multiple voltage sources, which can lead to overvoltage in one or more switches. The difficulty, however, can be remedied by using a voltage clamp or voltage control circuit. The majority of multilevel inverter research focuses on the modulation techniques used to control the power switching mechanisms. [4]

A prominent alternative multilevel inverter system with lower power devices is the cascaded H Bridge multilevel inverter, which is based on the series connection of H-bridges with different DC sources. In the five-level cascaded H-bridge multilevel inverter shown in Figure 4, the H-bridge output terminals are coupled in series, and the DC sources must be isolated from one another. Because of this property, CMIs have also been proposed for use with fuel cells or solar cell in order to achieve higher levels with lower total harmonic distortion. [8]

The voltages generated by separate H bridge cells are added to produce the final AC output voltage. The DC source is connected to the AC output via eight switches in various configurations. T_1, T_2, T_3, and T_4, the single phase H-bridge provides five voltage levels: $+E_{dc}/2$, $+E_{dc}/4$, 0, $-E_{dc}/4$, $-E_{dc}/2$. The CMI generates a five-level output voltage by combining two different DC sources per phase. To achieve $+E_{dc}$, turn on T_1 and T_4 switches, whereas to obtain $-E_{dc}$, turn on T_2 and T_3 switches or T_3 and T_4 switches.

If the number of modules connected in series is considered to be t, the number of output levels in each phase is q, as indicated in Equation 1 and Equation 2 can be used to identify the switching states of a CMI.

$$q = 2(t + 1) \tag{1}$$

$$SS = 3 * q \tag{2}$$

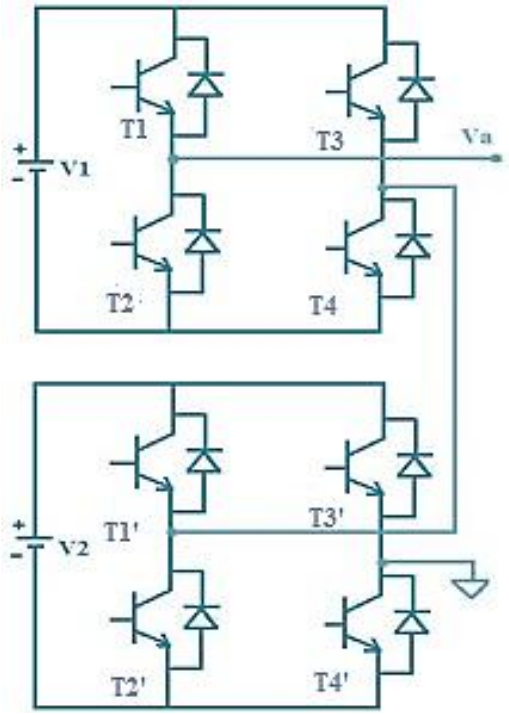


Figure 4 Representation of five levels cascaded H-Bridge inverter

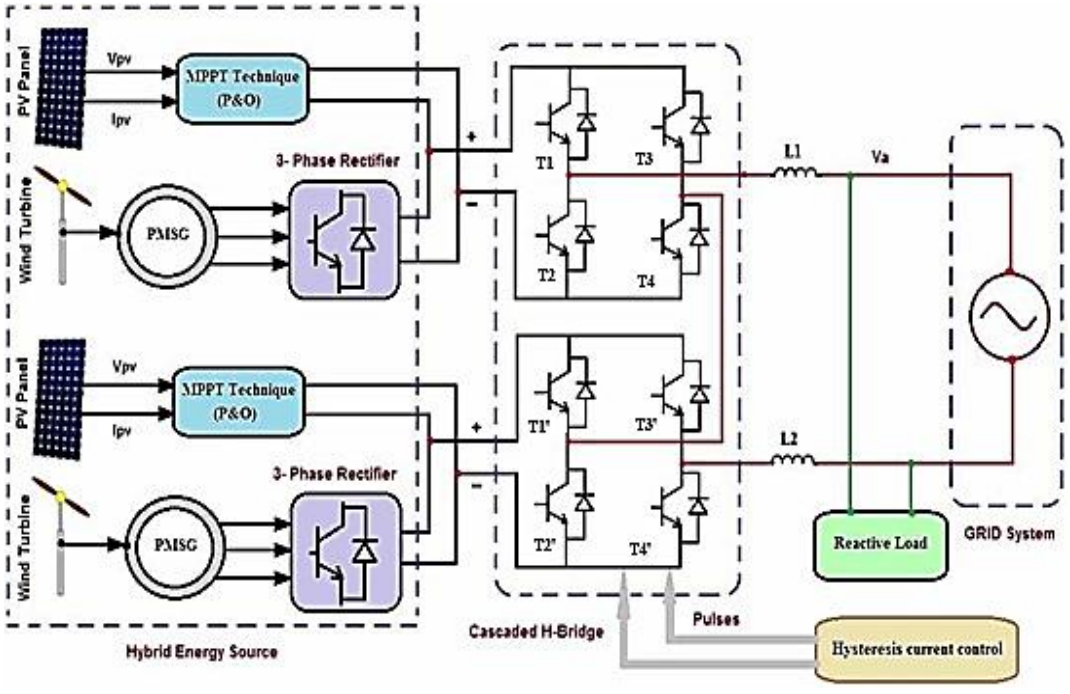


Figure 5 Block diagram of PV-Wind fed cascaded H-Bridge inverter with hysteresis control scheme

Figure 5 depicts the block diagram of proposed cascaded multilevel

inverter and the suggested control method. The PV-Wind hybrid energy sources are used to power the cascaded multilevel inverter. The maximum power of the PV array is tracked using the incremental conductance MPPT algorithm, which is combined with the voltage of the wind energy system via a 3-phase rectifier circuit. The CMI output is synced with a grid-connected system using a split inductor rather than a transformer, which eliminates the problem of leakage current and lowers the system's cost. To synchronize with any AC load, the split inductors L1 and L2 turn the staircase output into a pure sinusoidal waveform. To raise the planned system's power consumption, the reactive load is connected across the grid system. Using an upgraded hysteresis current control technique, the cascaded multilayer inverter is managed. [16]

ALGORITHM OF HYSTERSIS CURRENT CONTROL (HCC)

To generate the switching pulses for the multilevel inverter operation, the hysteresis current control space vector modulation approach was applied. Error computation, area detection, sector detection, and voltage vector selection are all processes in the hysteresis current control SVPWM.

Evaluation of the Hysteresis Band (h)

The goal of this system is to keep the current's real value inside their hysteresis band, which ranges from 0.1 to 0.9, at all times. The hexagonal hysteresis region is divided into 19 sectors by 27 switching state vectors. The actual current and reference current comparison covers the switching vector point in the hexagonal region depending on error current value. Figure 6 shows the hexagon representation of vectors in the proposed system. The variation hysteresis band value with variations in error current is used to compute the output voltage level of the proposed inverter. The output voltages are $-V_{dc}/2$, 0 and $V_{dc}/2$, dependent on the hysteresis band value variation. The output voltage is determined by the hysteresis band variation using the following Equations:

$$V = -\frac{Vdc}{2}, \text{ if } \Delta i > h1 \quad (3)$$

$$V = 0, \text{ if}(h1 < \Delta i < h2) \text{ or } (-h2 < \Delta i < -h1) \quad (4)$$

$$V = \frac{Vdc}{2}, \text{ if } \Delta i < h2 \quad (5)$$

where,

Δi - Hexagonal region area

H-hysteresis band value

The voltage levels are computed by taking the current error value $\Delta i = i_L - i_{Lref}$ into consideration and h1 and h2 hysteresis bands (upper and lower hysteresis bands). The hysteresis current control algorithm is a nonlinear control approach with high stability, fast dynamic response, intrinsic current-limiting capabilities and hysteresis band real-time regulation.

$$\text{Hysteresis band (h)} = \frac{V_a(V_{dc} - 2V_a)}{V_{dc}.L.f_s} \quad (6)$$

where,

V_a- Voltage reference

V_{dc} - DC input voltage

L-Value of split inductor

f_s- Switching frequency.

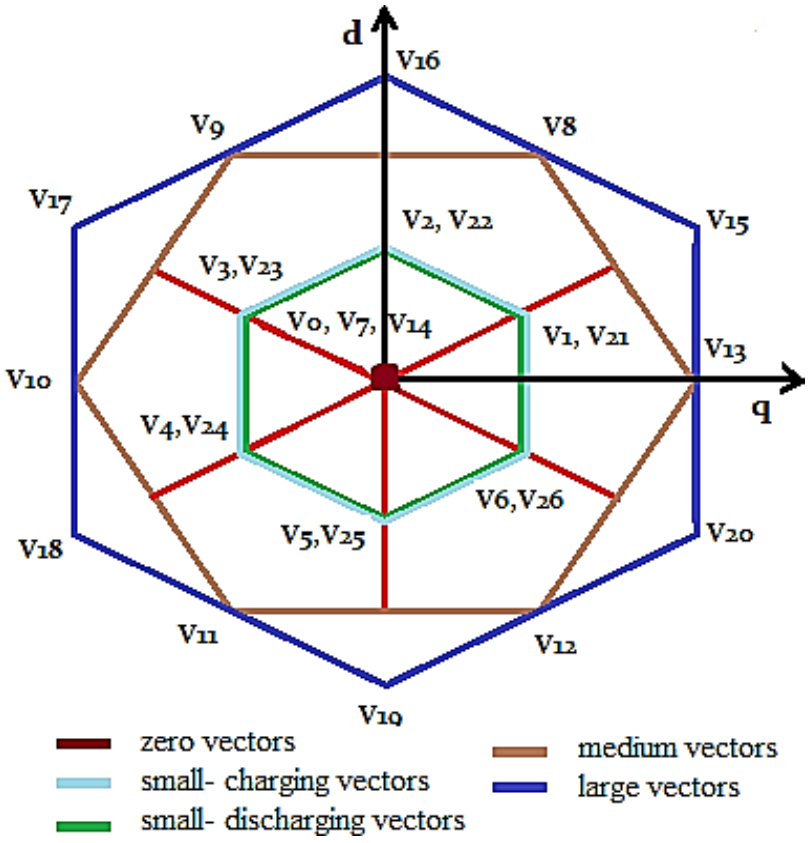


Figure 6 Representations of hexagonal vectors

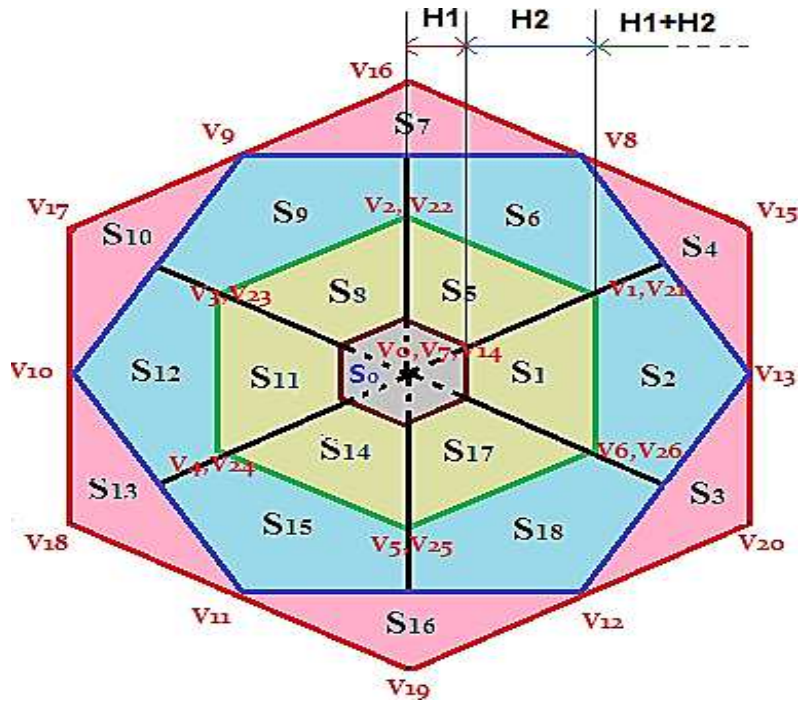


Figure 7 Representations of three hexagonal regions

Area Detection

Within the hysteresis bounds, the proposed hysteresis current control algorithm aims to keep the real load current near to the reference load current. The system is analyzed in the modified (α-β) frame and the three hysteresis bands are changed into this frame, resulting in three hexagon areas as illustrated in Figure 7. In order to exploit four categories of accessible voltage vectors, three hysteresis bands are chosen: zero, small, medium, and large. This arrangement makes the selection of an adequate voltage vector. [14]

The surface encompassed by the circle with radius h1 is defined as the first area I. The surface circumscribed by the two hexagons with radii h1 and h1+h2, respectively, is known as the second area-II. The region outside the hexagon of radius h1+h2 is the third area III. The h1 and h2 radii values are determined by the current reference value as well as the intended control dynamics. Because no zero voltage vectors are employed, the decision h1 = 0 may enhance the switching frequency. Furthermore, this option allows for a quick reaction from the load current control. To allow the neutral point voltage balancing by the employment of redundant space vectors, the radius h2 must be greater than zero ($h_2 > h_1 > 0$).

Vector components in a complex form can be used to express the reference load current i_{Lref} and the actual load current i_L,

$$i_{Lref} = i_{Lref\alpha} + j i_{Lref\beta} \quad (7)$$

$$i_L = i_{L\alpha} + j i_{L\beta} \quad (8)$$

In the same way, the error vector is defined as,

$$\Delta i = i_L - i_{Lref} \quad (9)$$

It is written as, in the reference frame.

$$\Delta i=\Delta i\alpha + \Delta i\beta \quad (10)$$

Sector Detection

The hysteresis bounds h1 and (h1 + h2) define regions RI and RII, respectively, but area A III has no upper limit (r > h1 + h2). Sector S0 is the sector represented by Region RI. S 1, S 4, S 10, S13, and S16 are the six sectors that make up Region II. As shown in Figure 8, the angle between any two consecutive sectors is 60 degrees. Sector S1, for example, is positioned between 30 and 30. S2, S3, S5, S6, S8, S11, S12, S14, S15, S17, and S18 are the 12 sectors that make up Region-III. The following two conditions govern the detection of the sector in which the present error vector's tip is located:

a) The sector in the hexagonal hysteresis area to which it is relevant.

b) The angle formed by the error vector Δi and the q axis parallel.

$$\theta i=\tan\left(\frac{\Delta i\beta}{\Delta i\alpha}\right) \quad (11)$$

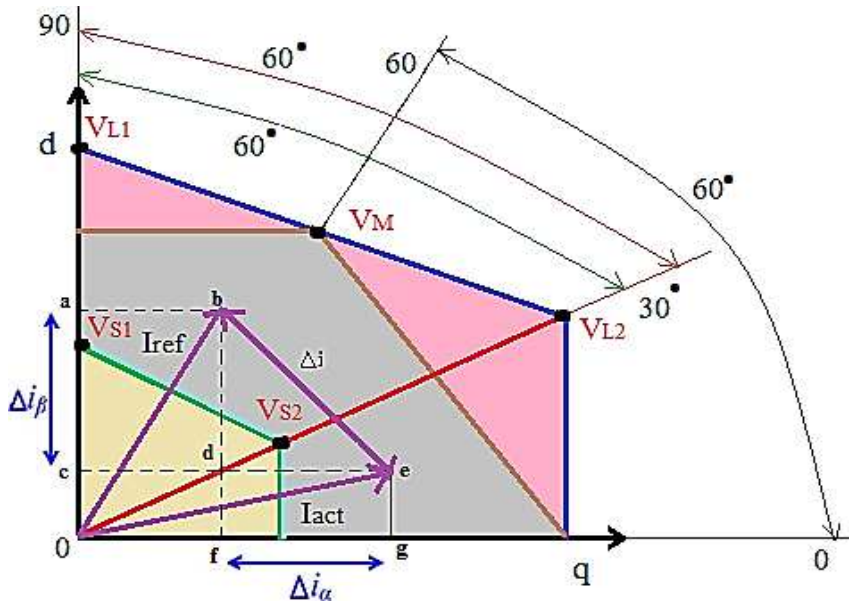


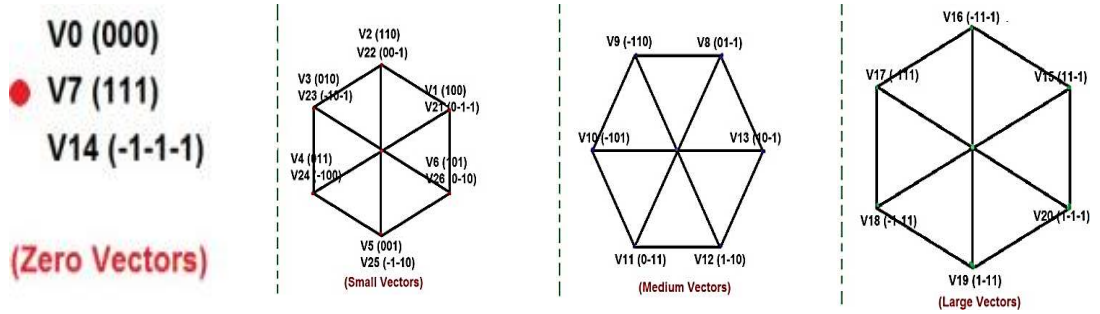
Figure 8 Representations of angle determination in hexagonal hysteresis current control algorithm

Depending on the angle value and the area number, the error vector tip can be found in any of the 19 sectors.

Voltage Vector Selection

Whenever the error-vector tip is in region RI (sector S0), the error is minimal and regarded acceptable for tracking current references within the needed accuracy. Then, with no connection, one of the three zero voltage vectors (V0, V7, or V14) is applied (Figure 9a). Similarly, if the error vector tip is in region RII, one of the small hexagon voltage vectors will be applied.

If the error vector tip is in any of sectors S3, S6, S12, S15, or S18 in the third region RIII, one of the medium hexagon voltage vectors will be chosen (Figure 9c). When the error-vector tip is positioned in one of the following sectors: S2, S5, S8, S11, S14, or S17 (Figure 9d), one of the large hexagon voltage vectors will be applied. The optimal voltage vector to transfer the error back toward the hysteresis region RI is either V4 or V24 if the error vector tip is located in sector S1 of region RII (Figure 9b). Figure 10 depicts the suggested Hysteresis current control flow chart method.



(a) **(b)** **(c)** **(d)**

Figure 9 Representations of area detection in hexagonal hysteresis current control algorithm (a) Region-I, (b) Region-II, (c) Region-IIIa and (d) Region-IIIb

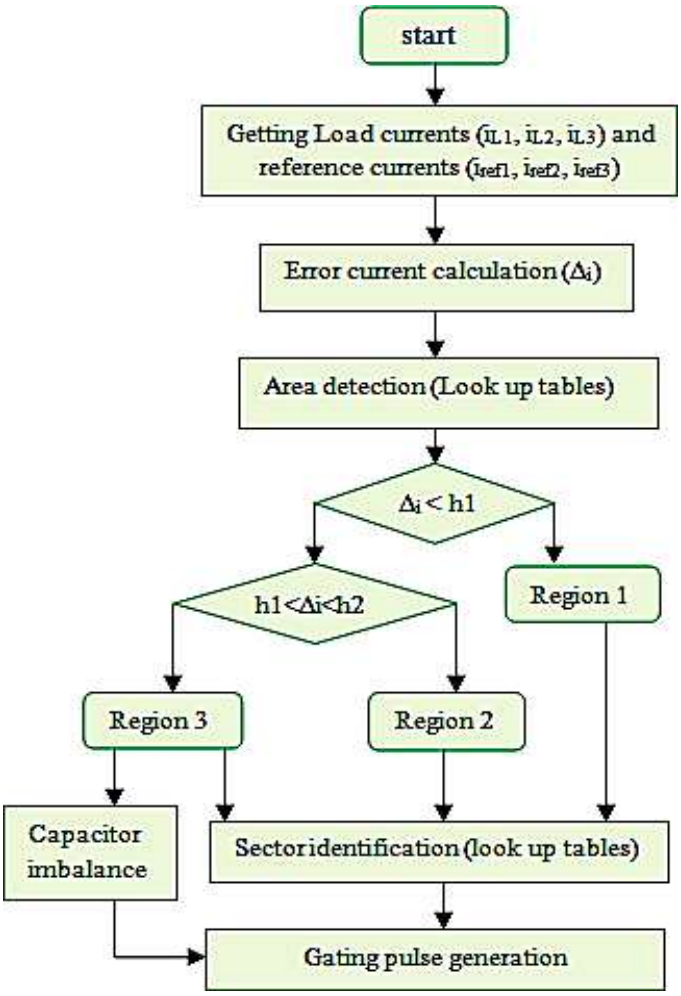
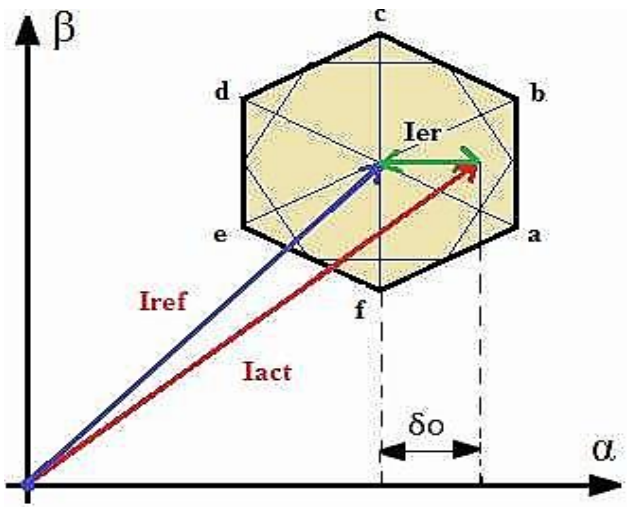


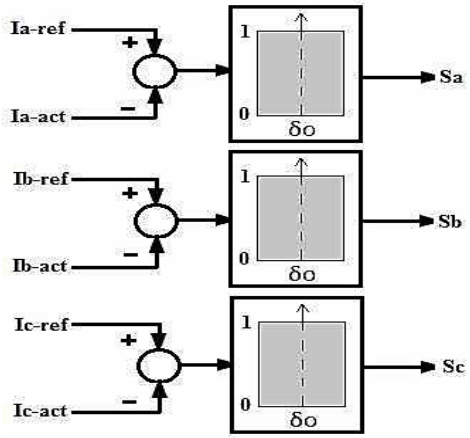
Figure 10 Flowchart of hysteresis current control algorithm

The number of bands around the reference vectors for hysteresis current regulation can be connected to the extent of inaccuracy for "n" inverter. The erroneous current value will determine the hysteresis bands h and h1, and the output voltage level of the proposed system will be dictated by the hysteresis band fluctuation. The error is determined by the difference between the actual current measured by the system and the reference current values.

Figures 11 (a) and 11 (b) illustrate the vector diagram of hysteresis current control and current calculation inaccuracy. The hysteresis current control is utilized to obtain output voltage levels of $+E_{dc}/2$, $+E_{dc}/4$, 0, $-E_{dc}/4$, and $-E_{dc}/2$ for a single phase, five-level cascaded inverter.



(a)



(b)

Figure 11 (a) Vector diagram of hysteresis current control and (b) System of error current calculation

Figure 12 depicts the output voltage generation for the proposed five-level CMI inverter system as the error current value varies. When it reaches point p, the voltage level is $-E_{dc}/4$. At this point, the voltage reaches its maximum in the negative range. The positive range of output voltage is obtained when the error current fluctuates from point s to point z. The output voltage of the proposed system reaches its maximum positive side at point w.

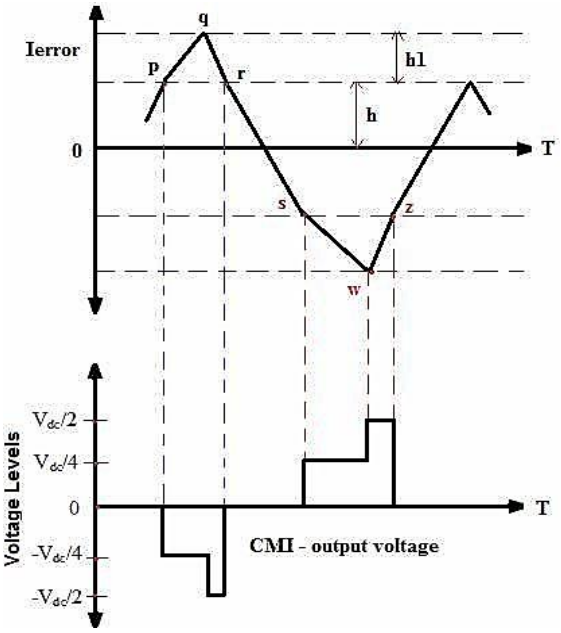


Figure 12 Hysteresis current control for cascaded multilevel inverter

SIMULATION AND EXPERIMENTAL RESULTS

The proposed system focuses on increasing the quality of power pumped into the grid. With the help of a 3-phase rectifier, the ac voltage from the permanent magnet synchronous generator is converted to dc and mixed with the dc output from the PV array, which receives solar irradiation ranging from 310W/m^2 to 1210W/m^2 and temperatures ranging from 0 to 42 degrees. Split inductors with a 4 mH are used to synchronize the inverter's stepped output with the grid characteristics.

The inverter side three phase current is measured, and the abc-dq conversion is applied using Park's transformation equation for closed loop current control. The three-phase reference current is added to the system via dq-abc transformation and hysteresis current control, and the hybrid source's reference current value is added.

Simulation Results

Figure 13 shows the PV array's DC output voltage of 81 V and current of 6.2 A. The rectified DC output voltage rectified by utilizing a 3-phase rectifier is shown in figure. 14. Another input source for the proposed system is a wind energy PMSG system, which creates a 150V ac output voltage when combined with the PV array voltage, as illustrated in Figure 15.

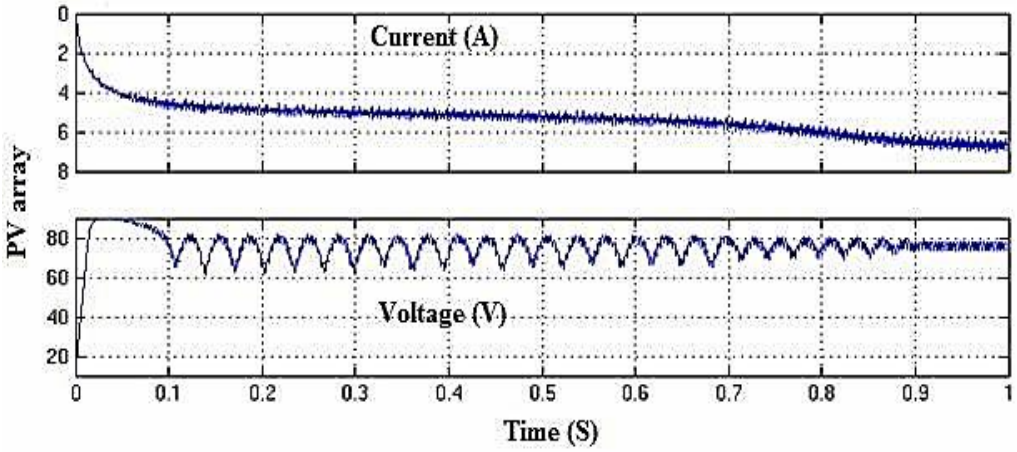


Figure 13 Photovoltaic current and voltage

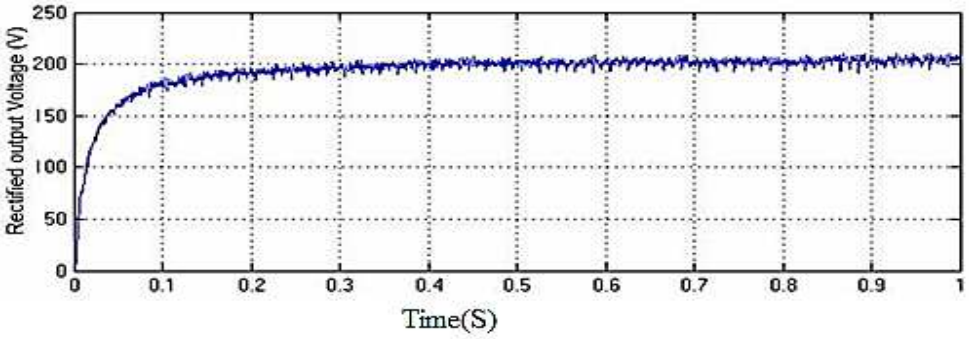


Figure 14 Rectified DC output voltage

Figure 16 shows how altering the hysteresis band from 0.11 to 0.955 improves the output voltage of the hysteresis controller in the suggested work. Figures 16 a and 16 b illustrate the output voltage of the proposed system with hysteresis bands of 0.1 and 0.4, respectively, while Figure 16 c shows the output voltage of 245.4V with a hysteresis band of 0.95, which is better than other

hysteresis band values.

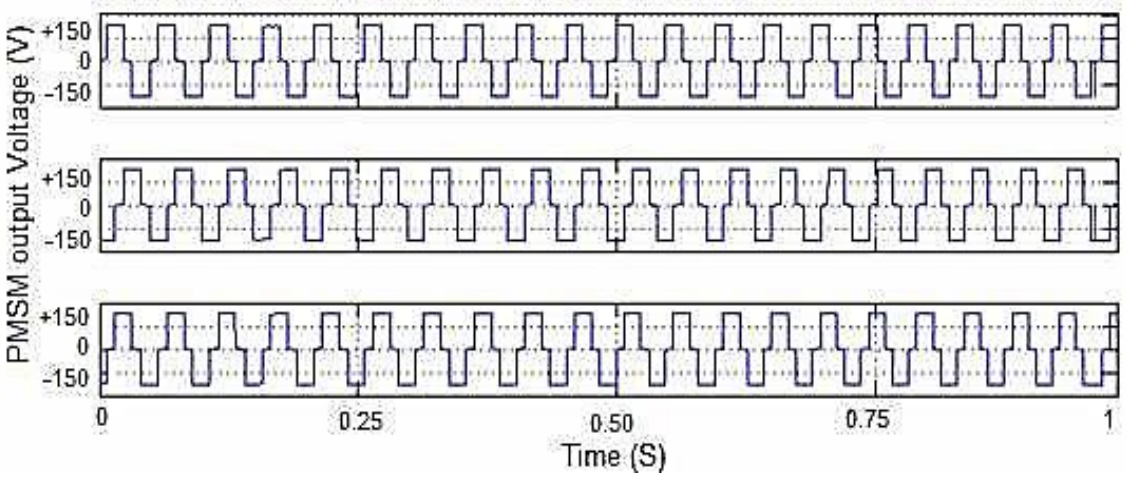
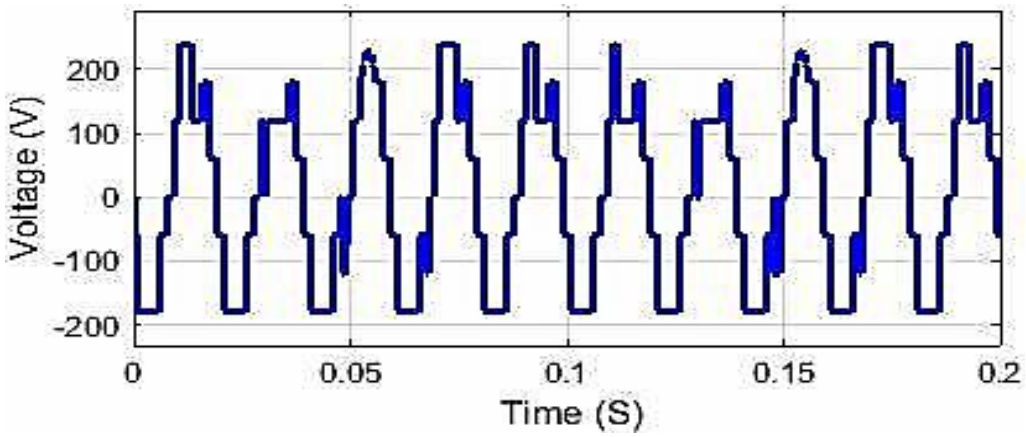
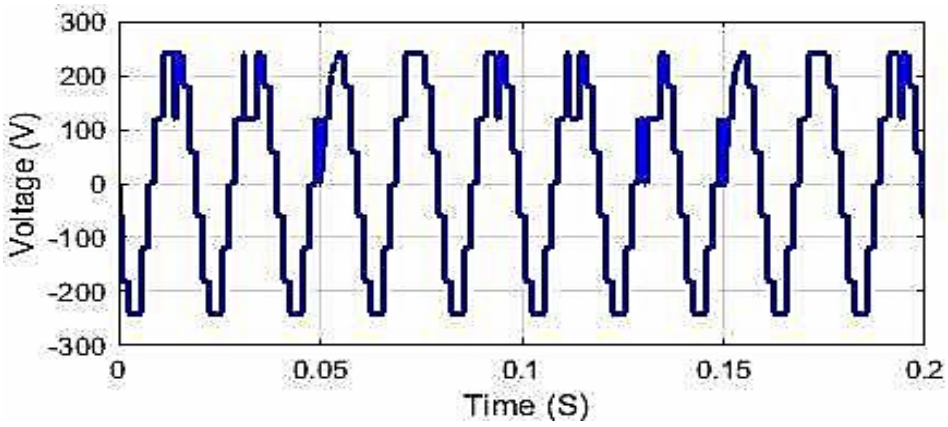


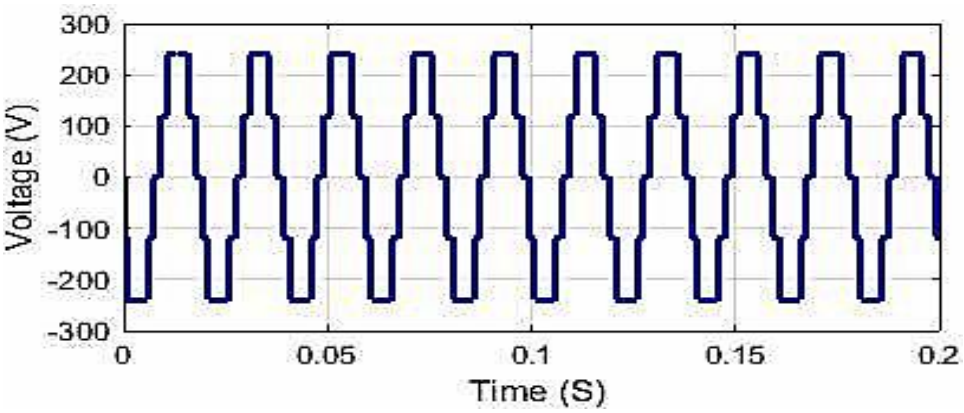
Figure 15 Output voltage of PMSG



(a)



(b)



(c)

Figure 16 Hysteresis band fluctuation in single phase H-Bridge inverter voltage (a) Hysteresis band=0.1 (b) Hysteresis band =0.4, (c) Hysteresis band =0.95

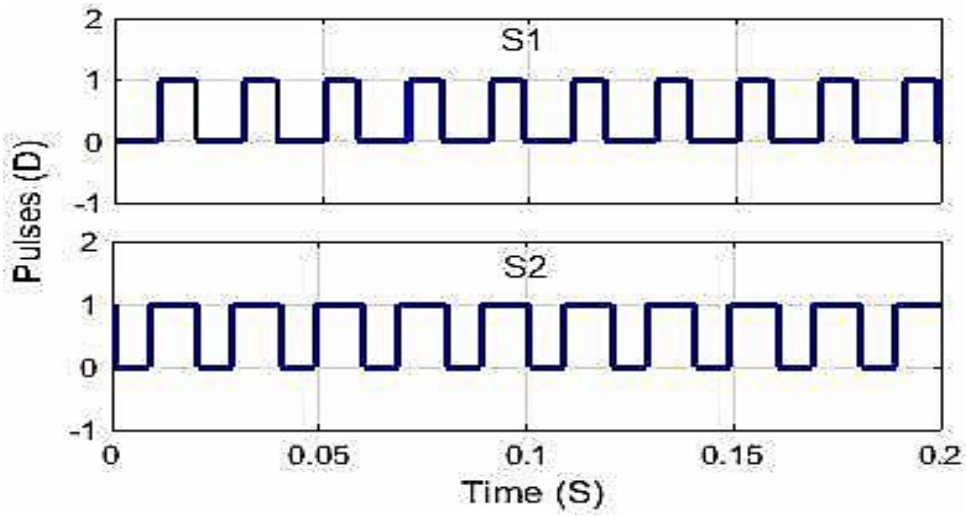
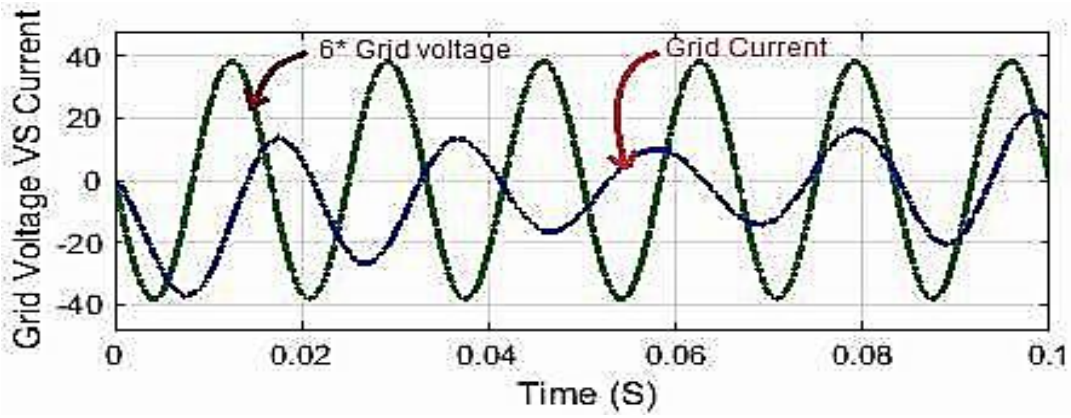
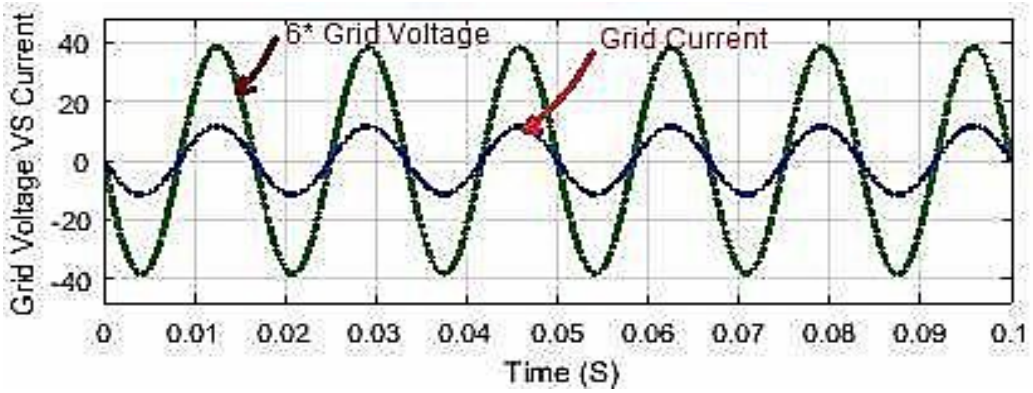


Figure 17 Gate pulses for H-bridge inverter switches S1&S2

Figure 17 shows the hysteresis current control-based switching pulses for S1 and S2 of the cascaded H-bridge inverter.



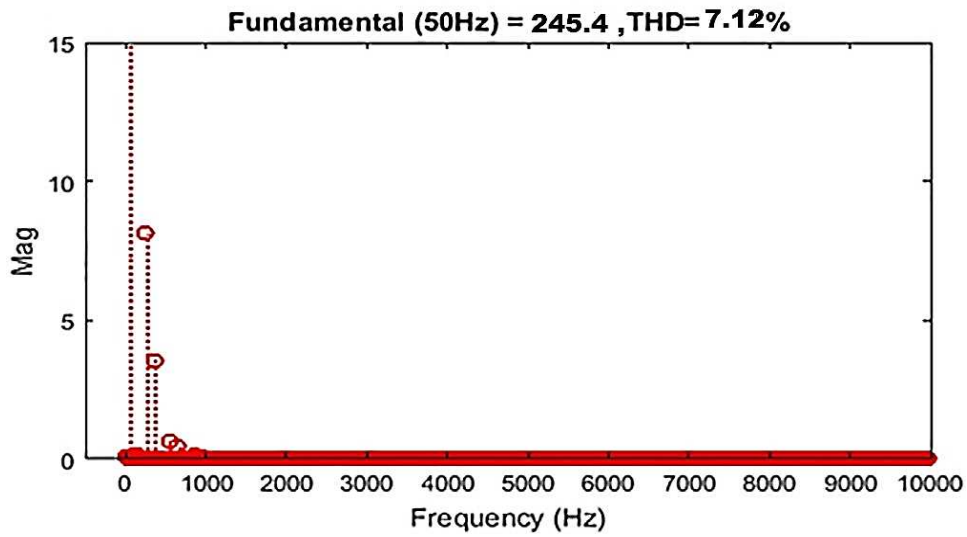
(a)



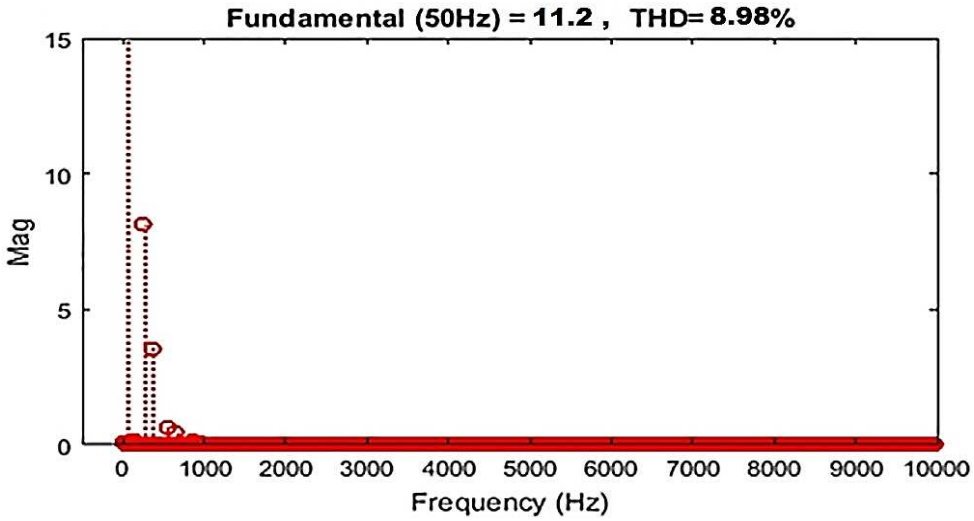
(b)

Figure 18 (a) Voltage & current synchronization for SPWM and (b) Voltage & current synchronization for Hysteresis Current Control (HCC)

Grid voltage and current synchronization for sinusoidal pulse width modulation and hysteresis current control are shown in Figures 18(a) and (b), respectively. Figure 19(a) and (b) illustrate the THD analysis of the proposed system for output voltage of 7.12 percent and current of 8.98 percent, respectively.



(a)



(b)

Figure 19 (a) Voltage THD and (b) Current THD

Figure 20 illustrates the simulation result of the common mode voltage, which is lowered to $V_{dc}/2$ times the applied DC input voltage and decreased to 122.7 V.

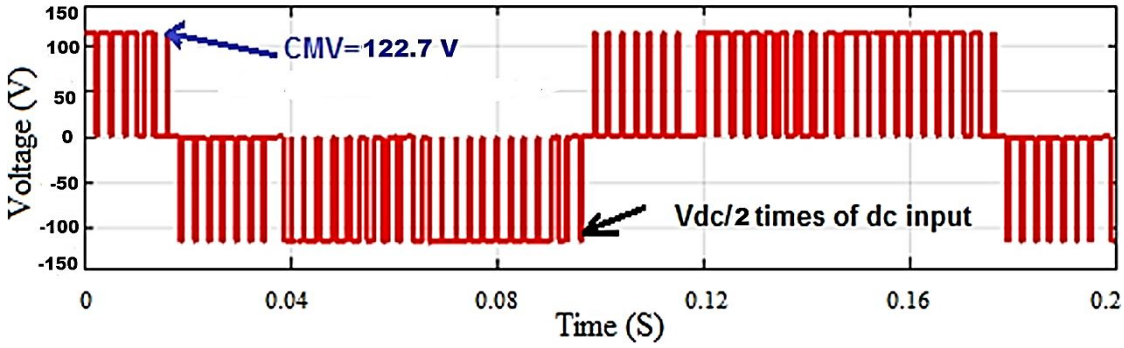


Figure 20 Simulation result of common mode voltage (CMV)

Table 1 CMV and THD comparison for various PWM topologies

PWM methods	CMV reduction	THD reduction (%)		Voltage boosting level
		Voltage	Current	
MSPWM	(V_{dc}/2)	9.6%	12.65%	1.1
Hysteresis current Control (HCC)	(V_{dc}/2)	7.12%	8.98%	1.5

Table 1 compares the various PWM approaches for THD, CMV ranges, and voltage boosting levels. In comparison to traditional PWM approaches, the proposed HCC method clearly outperforms them.

Experimental Results

To verify the modelling results of the proposed system, an experimental setup for hysteresis current control for photovoltaic-wind hybrid energy systems using a five-level cascaded inverter was built and tested. The ac voltage of the PMSG-wind energy system is converted to 148.1V dc using a 3-phase bride rectifier, then combined with the PV system voltage of 80.1V, which is fed to a cascaded h-bridge inverter.

On the inverter side, a stepped output of 238.45 V is obtained, and the THD is displayed in Figure 21. A sinusoidal voltage of 235.46V is created using split inductors and is synchronized with a single-phase grid connected system. The inverter legs were made up of IRF840 MOSFET switches, which had lower switching losses than traditional inverters, and the output waveforms were obtained using a Digital Storage Oscilloscope (DSO). The DSPIC30F microcontroller is used to implement hysteresis current regulation. Figure 22 illustrates the representation of common mode voltage, which is lowered to Vdc/2 times the applied DC input voltage and decreased to 122.7 V.

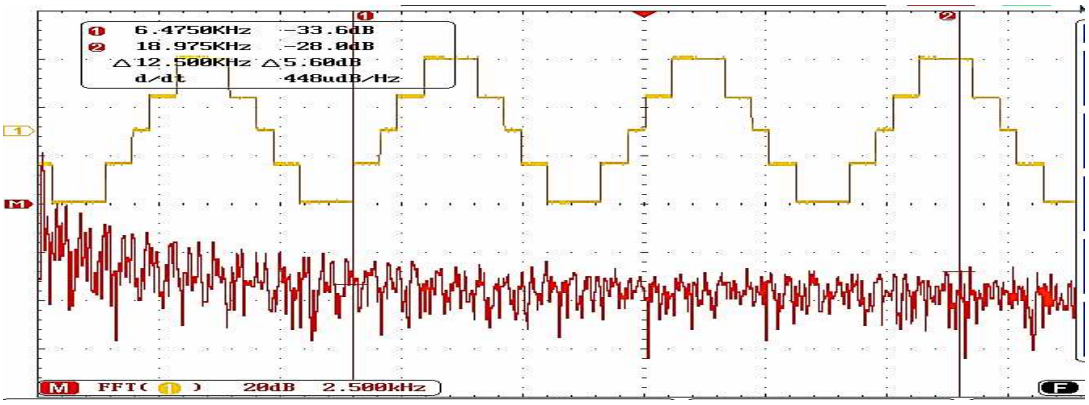


Figure 21 H-bridge inverter output voltage and THD analysis

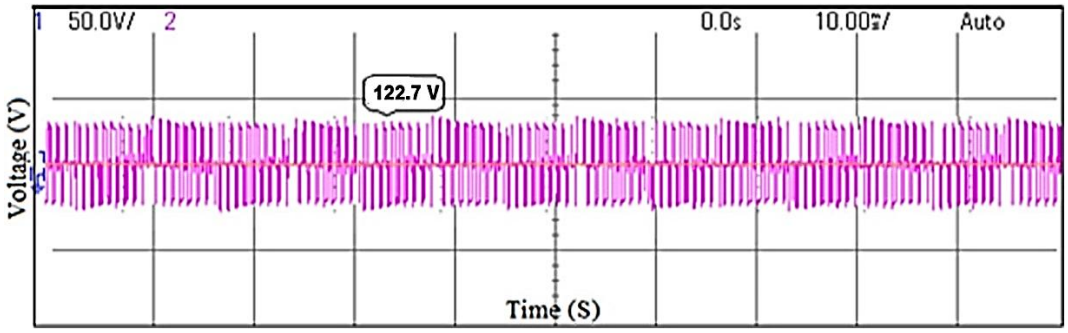


Figure 22 Representation of Common Mode Voltage (CMV)

CONCLUSION

This paper deals with the hysteresis current control algorithm for hybrid energy fed cascaded multilevel inverters. A modified variable step size

P&O MPPT algorithm has been given in this chapter, which can improve the PV system's dynamic and steady state performance at the same time. Traditional P&O MPPT has limitations, which are addressed by the suggested variable step size technique. The hysteresis current control algorithm is implemented for the cascaded multilevel inverter, which improves the inverter output voltage, minimizes the common mode voltage, which is lowered to $V_{dc}/2$ times the applied DC input voltage and decreased to 122.7 V, and minimizes the THD of output voltage of 7.12 percent and current of 8.98 percent, respectively. The proposed scheme was investigated through MATLAB/Simulink.

Data Availability: The data sets analyzed during the current study are not publicly available due to its own findings but are available from the corresponding author on reasonable request.

Clinical trial: Not applicable

Consent to Publish declaration: Not applicable

Ethics and Consent to Participate declarations: Not applicable

Author Contribution declaration:

Jayaprakasam Vinothini : Study conception and design

Ravindran Ramkumar: Material preparation, data collection and analysis

Ravi S : Draft of the manuscript was written

Research funding: No, this research did not receive funding

References

1. Pereda, J & Dixon, J 2013, 'Cascaded multilevel converters: Optimal asymmetries and floating capacitor control', in IEEE Transactions on Industrial Electronics, vol. 60, no. 11, pp. 4784-4793.
2. Raghu vamsi goutham, M & Venu Gopala Rao, M 2012, 'Control of a three-phase cascaded h-bridge multilevel inverter for stand-alone PV system', International Journal of Modern Engineering Research, vol. 2, no. 2, pp. 278-282.

3. Rahim, NA & Selvaraj, J 2010, ‘Multistring five-level inverter with novel PWM control scheme for PV application’, in IEEE Transactions on Industrial Electronics, vol. 57, no. 6, pp. 2111-2123.
4. Ravindran R, Sathiasamuel CR, Ramasamy P, Balasubramanian K. MSVM-based hybrid energy-fed quasi-Z-source cascaded H-bridge inverter for grid-connected system. Int Trans Electr Energ Syst. 2021;e13139. doi:10.1002/2050-7038.13139
5. Ning Zhu, Bin Wu, Deiwei (David) Xu, Navid & Zargari, R 2011, ‘Common-mode voltage reduction methods for medium-voltage current source inverter- fed drives’, IEEE Energy Conversion Congress and Exposition, pp. 3136-3143, DOI: 10.1109/ECCE.2011.6064191.
6. R. Ramkumar, M. V. Kumar and D. Sivamani, "Fuzzy Logic based Soft Switched Active Clamped Boost Converter Charging Strategy for Electric Vehicles," 2020 4th International Conference on Electronics, Communication and Aerospace Technology (ICECA), 2020, pp. 1334-1339, doi: 10.1109/ICECA49313.2020.9297422.
7. Nikita Kshirsagar, Debre, PD, Akshay Kadu & Rahul Juneja 2017, ‘Design of three phase z-source inverter for solar photovoltaic application’, in International Conference on Innovations in information Embedded and Communication Systems (ICIIECS), pp. 1-6, DOI: 10.1109/ICIIECS. 2017.8276108.
8. S. Sathish Kumar, R. Ramkumar, S. Sivarajeswari, D. Ramya, T. Subburaj, Martin Sankoh, "Performance Enhancement of a Three Phase Boost-Cascaded Fifteen Level Inverter Using the PI Controller", Mathematical Problems in Engineering, vol. 2022, Article ID 3888571, 17 pages, 2022. https://doi.org/10.1155/2022/3888571.
9. R. Ramkmar and A. A. Vikram, "Wind energy based asymmetrical half bridge flyback converter for BLDC motor," 2017 Third International Conference on Science Technology Engineering & Management (ICONSTEM), Chennai, 2017, pp. 605-610, doi: 10.1109/ICONSTEM.2017.8261394
10. S. Sathish Kumar, R. Ramkumar al 2022, "Design and Control of modified Resonant voltage multiplier rectifier for Photovoltaic applications using electrolytic capacitive material”, JournalNanomaterials, vol.2022, ArticleID 1151408,11 pages, 2 022. https://doi.org/10.1155/2022/1151408.
11. Wang, J, Jin, J, Abu-Siada, A & Zheng, L 2020, ‘Sliding mode SVPWM current control for shunt active power filter’, IEEE International Conference on Applied Superconductivity and Electromagnetic Devices (ASEMD), pp. 1-2, DOI: 10.1109/ASEMD49065.2020.9276260.
12. D. Ramya, R. Ramkumar, A. Tamilselvan, VS. Jagadesh “High efficiency bridgeless single power conversion battery charger for electric vehicle”, Materials Today: Proceedings,2022, ISSN 2214-7853, https://doi.org/10.1016/j.matpr.2022.05.147.

13. Le, QA & Lee, D 2019, 'Elimination of common-mode voltages based on modified SVPWM in five-level ANPC inverters', in IEEE Transactions on Power Electronics, vol. 34, no. 1, pp. 173-183. DOI: 10.1109/TPEL.2018. 2825230.
14. Saurabh Gupta, R. Ramkumar, M. Lakshmi, M. Vinoth kumar, R. Surendar, N. Mayavel, "Soft switched DC-DC converter for hybrid power generation photo voltaic panels using fuzzy logic controller", Materials Today: Proceedings,2022, ISSN 2214-7853, https://doi.org/10.1016/j.matpr.2022.05.146.
15. Lopez, Ó, Alvarez, J, Doval-Gandoy, J & FD, Freijedo 2008, 'Multilevel multiphase space vector PWM algorithm', in IEEE Transactions on Industrial Electronics, vol. 55, no. 5, pp. 1933-1942, DOI:10.1109/TIE. 2008.918466.
16. Ramkumar, R., et al2019. Intelligent system to monitor and diagnose performance deviation in Industrial Equipment.IOPconf.Series:Materials science and Engineering 623(2019)012012.
17. Krithiga, S & Ammasai Gounden, N 2014, 'Investigations of an improved PV system topology using multilevel boost converter and line commutated inverter with solutions to grid issues', Simulation Modelling Practice and Theory, vol. 42, pp. 147-159.
18. Mohseni, M & Islam, SM 2010, 'A new vector-based hysteresis current control scheme for three-phase PWM voltage-source inverters', in IEEE Transactions on Power Electronics, vol. 25, no. 9, pp. 99-2309, DOI: 10.1109/TPEL.2010.2047270.
19. McGrath, BP, Holmes, DG & Meynard, T 2006, 'Reduced PWM harmonic distortion for multilevel inverters operating over a wide modulation range', in IEEE Transactions on Power Electronics, vol. 21, no. 4, pp. 941-949, DOI: 10.1109/TPEL.2006.876864.
20. Yuyao He, Yuhao Xu & Jinping Chen 2018, 'New space vector modulation strategies to reduce inductor current ripple of z-source inverter', IEEE Transactions on Power Electronics, vol. 33, no. 3, pp. 2643-2654.